N2 O rate of change as a diagnostic of the Brewer-Dobson Circulation in the stratosphere

Daniele Minganti[1,1], Simon Chabrillat[1,1], Quentin Errera[1,1], Maxime Prignon[2,2], Douglas E Kinnison[3,3], Rolando R Garcia[3,3], Marta Abalos[4,4], Justin Alsing[5,5], Matthias Schneider[6,6], Dan Smale[7,7], Nicholas Jones[8,8], and Emmanuel Mahieu[9,9]

[1]Royal Belgian Institute for Space Aeronomy
[2]Chalmers University of Technlogy
[3]National Center for Atmospheric Research
[4]Universidad Complutense de Madrid
[5]Oskar Klein Centre for Cosmoparticle Physics, Department of Physics, Stockholm University
[6]Karlsruhe Institute of Technology
[7]NIWA Lauder
[8]University of Wollongong
[9]University of Liège

December 7, 2022

Abstract

The Brewer-Dobson Circulation (BDC) determines the distribution of long-lived tracers in the stratosphere; therefore, their changes can be used to diagnose changes in the BDC. We investigate decadal (2005-2018) trends of nitrous oxide (N2O) stratospheric columns (12-40 km) as measured by four Fourier transform infrared (FTIR) ground-based instruments and by the Atmospheric Chemistry Experiment Fourier Transform Spectrometer (ACE-FTS), and compare them with simulations by two models: a chemistry-transport model (CTM) driven by four different reanalyses, and the Whole Atmosphere Chemistry-Climate Model (WACCM). The limited sensitivity of the FTIR instruments can hide negative N2O trends in the mid-stratosphere because of the large increase in the lowermost stratosphere. When applying the ACE-FTS sampling on model datasets, the reanalyses by the European Centre for Medium Range Weather Forecast (ECMWF) compare best with ACE-FTS, but the N2O trends are consistently exaggerated. Model sensitivity tests show that while decadal N2O trends reflect changes in transport, these trends are less significant in the northern extratropics due to the larger variability of transport over timescales shorter than two years in that region. We further investigate the N2O Transformed Eulerian Mean (TEM) budget in three model datasets. The TEM analysis shows that enhanced advection affects the stratospheric N2O trends more than changes in mixing. While no ideal observational dataset currently exists, this model study of N2O trends still provides new insights about the BDC and its changes thanks to relevant sensitivity tests and the TEM analysis.

Evaluation of the N_2O rate of change to understand the stratospheric Brewer-Dobson Circulation in a Chemistry-Climate Model

Daniele Minganti [1], Simon Chabrillat [1], Quentin Errera [1], Maxime Prignon [2*], Douglas E. Kinnison [3], Rolando R. Garcia [3], Marta Abalos[4], Justin Alsing[5,9], Matthias Schneider [6], Dan Smale [7], Nicholas Jones [8], Emmanuel Mahieu [2]

[1]Royal Belgian Institute for Space Aeronomy, BIRA-IASB, Brussels, Belgium
[2]Institute of Astrophysics and Geophysics, UR SPHERES, University of Liège, Liège, Belgium
[3]National Center for Atmospheric Research, Boulder, CO, USA
[4]Universidad Complutense de Madrid, Madrid, Spain
[5]Oskar Klein Centre for Cosmoparticle Physics, Department of Physics, Stockholm University, Stockholm SE-106 91, Sweden
[6]Institute of Meteorology and Climate Research (IMK-ASF), Karlsruhe Institute of Technology, Karlsruhe, Germany
[7]National Institute of Water and Atmospheric Research, Lauder, New Zealand
[8]School of Chemistry, University of Wollongong, Wollongong, Australia
[9]Imperial Centre for Inference and Cosmology, Department of Physics, Imperial College London, Blackett Laboratory, Prince Consort Road, London SW7 2AZ, UK

Key Points:

- Sparse sampling of Atmospheric Chemistry Experiment Fourier Transform Spectrometer exaggerates the stratospheric nitrous oxide trends
- Transformed Eulerian Mean analysis shows that the residual mean advection contributes to the positive nitrous oxide trend in the Tropics
- The Whole Atmosphere Community-Climate Model simulates weaker hemispheric asymmetries of the nitrous oxide trends compared to reanalyses

*Currently at: Department of Earth, Space and Environment, Chalmers University of Technology, 41296, Gothenburg, Sweden

Corresponding author: Daniele Minganti, daniele.minganti@aeronomie.be

Abstract

The Brewer-Dobson Circulation (BDC) determines the distribution of long-lived tracers in the stratosphere; therefore, their changes can be used to diagnose changes in the BDC. We evaluate decadal (2005-2018) trends of nitrous oxide (N_2O) in two versions of the Whole Atmosphere Chemistry-Climate Model (WACCM) by comparing them with measurements from four Fourier transform infrared (FTIR) ground-based instruments, the Atmospheric Chemistry Experiment Fourier Transform Spectrometer (ACE-FTS), and with a chemistry-transport model (CTM) driven by four different reanalyses. The limited sensitivity of the FTIR instruments can hide negative N_2O trends in the mid-stratosphere because of the large increase in the lowermost stratosphere. When applying ACE-FTS measurement sampling on model datasets, the reanalyses from the European Centre for Medium Range Weather Forecast (ECMWF) compare best with ACE-FTS, but the N_2O trends are consistently exaggerated. The N_2O trends obtained with WACCM disagree with those obtained from ACE-FTS, but the new WACCM version performs better than the previous above the Southern Hemisphere in the stratosphere. Model sensitivity tests show that the decadal N_2O trends reflect changes in the stratospheric transport. We further investigate the N_2O Transformed Eulerian Mean (TEM) budget in WACCM and in the CTM simulation driven by the latest ECMWF reanalysis. The TEM analysis shows that enhanced advection affects the stratospheric N_2O trends in the Tropics. While no ideal observational dataset currently exists, this model study of N_2O trends still provides new insights about the BDC and its changes because of the contribution from relevant sensitivity tests and the TEM analysis.

Plain Language Summary

The circulation in the stratosphere is characterized by upward motion above the Tropics, followed by poleward and downward motions above the high latitudes. Changes in the pattern of this stratospheric circulation are currently a challenging topic of research. We investigate the decennial changes of this stratospheric circulation using observations and numerical simulations of the long-lived tracer nitrous oxide. Observations are obtained from ground-based and satellite instruments. Numerical simulations include complex atmospheric models that reproduce the chemistry and dynamics of the stratosphere. Both observations and models show differences between the hemispheres in the nitrous oxide decennial changes. Unfortunately, the current observations of nitrous oxide are not perfect. The ground-based instruments cannot correctly measure the changes of nitrous oxide in the northern hemisphere. The satellite does not measure at all times, and it spatially covers more the high latitudes, which negatively affects the measurements of nitrous oxide. On the other hand, model simulations can provide valuable insights into the changes in the stratospheric circulation. They show that changes in the stratospheric circulation cause the differences between hemispheres in the nitrous oxide trends and show that the circulation changes can be associated with different physical processes.

1 Introduction

Nitrous oxide (N_2O) is continuously emitted in the troposphere, with a nearly constant rate of change of 2% per decade, and transported into the stratosphere, where it is destroyed by photodissociation mainly in the Tropics above 35 km (Tian et al., 2020). The atmospheric lifetime of N_2O is approximately 120 years, which makes it an excellent tracer for stratospheric transport studies (Seinfeld & Pandis, 2016). Within the stratosphere, the lifetime of N_2O depends also on the solar activity because of its influence on the photolysis rates, with slightly decreased lifetime during solar maxima and increased lifetime during solar minima (Prather et al., 2015).

N_2O enters the stratosphere in the Tropics, and is transported towards higher latitudes by the Brewer-Dobson Circulation (BDC, Dobson et al., 1929; Brewer, 1949; Dobson, 1956). The BDC is driven by the breaking of tropospheric waves that propagate into the stratosphere (e.g., Charney & Drazin, 1961) and is often separated into an advective component, the residual mean meridional circulation (hereafter residual circulation), and a mixing component (Garny et al., 2014). The residual circulation consists in upwelling in the Tropics, followed by poleward flow and downwelling over the middle and high latitudes (Plumb, 2002). The mixing is a two-way exchange of mass that, within the stratosphere, occurs mostly on isentropic surfaces, thus, it is mainly quasi-horizontal (Shepherd, 2007). The BDC has a significant impact in determining the stratospheric distribution of chemical tracers, like ozone and greenhouse gases (e.g., Butchart, 2014), and in maintaing the observed meridional and vertical temperature structure of the stratosphere (Holton, 2004). Long-term changes in the BDC can have significant impacts on the climate system. One of the most important is the effect on the recovery of stratospheric ozone, as a changing BDC would result in changes of its meridional distribution (e.g., Shepherd, 2008; Dhomse et al., 2018). Changes in the BDC also impact the lifetime of Ozone Depleting Substances (ODS) in the stratosphere (Butchart & Scaife, 2001; Waugh & Hall, 2002), as well as the water vapor entering the stratosphere through the Tropics (e.g., Randel & Park, 2019). The troposphere is also affected by BDC changes because of the impact on the mass exchange with the stratosphere (e.g., ozone, Meul et al., 2018), and on the ultra-violet radiation reaching the surface (Meul et al., 2016).

Given the relevance of the BDC changes, understanding them is thus fundamental to fully comprehend the past and future evolution of climate. Simulations by Chemistry-Climate Models (CCMs) robustly project an acceleration of the BDC throughout the stratosphere in recent and coming decades due to the increase of greenhouse gases (e.g., Abalos et al., 2021). On the other hand, Oberländer-Hayn et al. (2016) argue that the global BDC trends in the lower stratosphere in CCMs are caused to a large extent by a lift of the tropopause level in response to global warming rather than an actual speedup of the circulation. Another significant impact of the increase of greenhouse gases is the shrinkage of the stratosphere, i.e., the combination of the tropopause rise and the downward shift of the height of the pressure levels above 55 km, that results from its cooling over the last decades (Pisoft et al., 2021). Modelling studies have shown that this stratospheric shrinking can impact the BDC and modulate its changes over the past decades (Šácha et al., 2019; Eichinger & Šácha, 2020). Such modulation consists in a BDC acceleration similar to that resulting from the impact of the tropopause lift (Eichinger & Šácha, 2020). In addition, CCMs simulations show that also the vertical and meridional structure of the BDC has changed in the past decades in response to climate change (Hardiman et al., 2014). Other modeling studies have shown that mixing, both on resolved and unresolved scales, also plays an important role in the simulated magnitudes of the BDC changes in addition to changes in the residual circulation among CCMs (e.g., Eichinger et al., 2019). Recent studies have also shown that ODS, through their impact on ozone, play a significant role in the modeled BDC changes (Abalos et al., 2019). In particular, the ODS decrease resulting from the Montreal Protocol, will reduce the global warming-induced acceleration of the BDC and potentially lead to hemispheric asymmetries in the BDC trends (Polvani et al., 2019).

The BDC and its changes cannot be measured directly (e.g., Minschwaner et al., 2016), but can be indirectly examined from measurements of stratospheric long-lived tracers (e.g., Engel et al., 2009; Hegglin et al., 2014) or temperature (Fu et al., 2015). Recently, Strahan et al. (2020) used ground-based observations of nitric acid and hydrogen chloride to investigate hemispheric-dependent BDC changes in the stratosphere. Similarly, space-borne observations of stratospheric tracers are often used to investigate decadal changes in the BDC using, e.g., hydrogen fluoride (Harrison et al., 2016), ozone (Nedoluha et al., 2015) or N_2O (Han et al., 2019). Measurements of stratospheric tracers are often used to calculate the mean Age of Air (AoA, Hall & Plumb, 1994). The mean AoA is a widely used diagnostic for stratospheric transport and is defined as the transit time of an air parcel from the tropical tropopause (or the surface, depending on the definition) to a certain point of the stratosphere (Waugh & Hall, 2002). Engel et al. (2017) used balloon-borne observations of carbon dioxide and methane to derive mean AoA trends above the northern mid-latitudes in the mid-lower stratosphere. Engel et al. (2017) found positive but not statistically significant mean AoA trends over about 40 years (corresponding to a possible slowdown of the BDC), which is in contrast with the modeling studies that simulate a significant acceleration of the BDC over the same region (e.g., Abalos et al., 2021). These discrepancies can be partly attributed to the temporal and spatial sparseness of the measurements and to uncertainties in the mean AoA trends derived from real tracers (Garcia et al., 2011; Fritsch et al., 2020). In addition to ground-based measurements, space-borne observations have been used to compute mean AoA trends as well (e.g., Stiller et al., 2012; Haenel et al., 2015). These observational studies using remote sensing measurements have shown a hemispheric asymmetry in the mean AoA trends over 2002-2012, with positive changes in the Northern Hemisphere (NH) and negative changes in the Southern Hemisphere (SH) (e.g., Mahieu et al., 2014; Stiller et al., 2017). The mean AoA indirectly obtained from satellite measurements in these studies does not allow the separation between residual circulation and mixing, which was proven to be important in CCMs (Dietmüller et al., 2018). However, Linz et al. (2021) showed that the effect of mixing can be explicitly calculated using AoA vertical gradients from both models and satellite measurements. In addition, von Clarmann and Grabowski (2021) (similarly to the early study of Holton & Choi, 1988) proposed an alternative method to infer the stratospheric circulation from satellite measurements of long-lived tracers by a direct inversion of the continuity equation.

Reanalysis datasets try to fill the gap between observations and free-running models, providing a global multi-decadal and continuous state of the past atmosphere by assimilating available observations. Dynamical fields from reanalyses can be used to drive Chemistry-Transport Models (CTMs) to simulate the distribution of real and synthetic tracers in the atmosphere. In the past decade, these CTM experiments have been used to investigate BDC changes in reanalyses using the AoA diagnostic (e.g., Monge-Sanz et al., 2012; Diallo et al., 2012; Ploeger et al., 2015). However, significant differences exist in the BDC changes obtained from different reanalyses, both over multi-decadal and decadal time scales (e.g., Abalos et al., 2015; Chabrillat et al., 2018). Furthermore, the computation of mean AoA largely depends on whether the kinematic velocities or the heating rates are used to drive the CTMs, leading to significant differences within the same reanalysis (Ploeger et al., 2019).

This study is based on the work performed by Minganti et al. (2020, hereafter M2020), who evaluated the climatological BDC in the Whole Atmosphere Community Climate Model (WACCM) version 4 (Garcia et al., 2017). The evaluation in M2020 consisted in studying the impact of the BDC on the climatologies of the stratospheric N_2O abundancies and of the N_2O Transformed Eulerian Mean (TEM) budget (Andrews et al., 1987). This evaluation was performed by comparison with simulations of the Belgian Assimilation System for Chemical ObsErvation Chemistry-Transport Model CTM (BASCOE CTM, Chabrillat et al., 2018) driven by dynamical reanalyses and with the BASCOE reanalysis of Aura Microwave Limb Sounder (MLS) version 2 (BRAM2, Errera et al., 2019). The TEM diagnostic was included in M2020 because it allows separating the effects of transport and chemistry on the rate of change of a stratospheric tracer such as N_2O (Randel et al., 1994). Within the TEM framework, the impact of transport can be further separated into the impact from the residual circulation and mixing, as was done for ozone and carbon monoxide in Abalos et al. (2013). It is important to note that the mixing obtained from the TEM analysis generally includes contributions from advective transport that are not represented by the residual circulation (Holton, 2004). After studying the climatologies in M2020, the present study aims to evaluate the changing BDC in WACCM in its versions 4 and 6 (Gettelman et al., 2019) by studying multi-decadal and decadal changes of N_2O in the stratosphere, comparing them with ground-based and space-borne observations and BASCOE CTM simulations. We also evaluate the changes in TEM N_2O budget in WACCM and in the BASCOE CTM. We compare the model simulations with ground-based observations of N_2O from Fourier transform infrared (FTIR) spectrometers that are part of the Network for the Detection of Atmospheric Composition Change (NDACC) at four stations in the SH and NH subtropics as well as at mid-latitudes (De Mazière et al., 2018, `http://www.ndaccdemo.org/`). We also use satellite measurements from the Atmospheric Chemistry Experiment Fourier Transform Spectrometer (ACE-FTS, Bernath et al., 2021). Contrary to M2020, we cannot use N_2O from BRAM2 because of the unrealistic negative drift in the MLS N_2O dataset (Livesey et al., 2021). The BASCOE CTM is driven by four modern reanalyses that are part of the SPARC (Stratosphere-troposphere Processes and their Role in Climate) Reanalysis Intercomparison Project (S-RIP, Fujiwara et al., 2017).

The present study is structured as follows. Section 2 describes the observational and modeling datasets used in this study, as well as the TEM diagnostics and the regression model used to derive linear trends. In Section 3, we use FTIR observations to evaluate the trends in the stratospheric N_2O columns obtained from WACCM and the CTM simulations and from satellite measurements. In Section 4, using ACE-FTS as a reference, we study the global N_2O trends in the stratosphere and focus on the differences in the trend patterns among datasets. In Section 5, we investigate the N_2O TEM budget from WACCM version 6 and a BASCOE simulation in order to separate the impact of the residual circulation and mixing on the N_2O trends. Finally, Section 6 concludes the study with a summary of the principal findings.

2 Data and Methods

This section describes the observational and model data as well as the methods used in this study (see Tables 1 and 2). Throughout the study, we will refer to the CCMs and the BASCOE CTM simulations as "models" to distinguish them from the observations obtained from the FTIR and ACE-FTS. For the sake of brevity, we refer to M2020 for a more detailed description of the dataset (BASCOE CTM, WACCM version 4, and S-RIP reanalyses) and methods (TEM framework) already used there.

Dataset name	Full Name	Reference	Year range	Vert. resol. + top
WACCM-REFC1	Whole Atmosphere Community Climate Model	Marsh et al. (2013) Garcia et al. (2017)	1985-2018	L66, 5.96 10^{-6} hPa
WACCM-REFD1	Whole Atmosphere Community Climate Model	Gettelman et al. (2019)	1985-2018	L70, 5.96 10^{-6} hPa
CTM+ERAI	ECMWF Reanalysis Interim	Dee et al. (2011)	1985-2018	L60, 0.1 hPa
CTM+ERA5	ECMWF Reanalysis 5	Hersbach et al. (2020)	1985-2019	L86, 0.01 hPa
CTM+JRA55	Japanese 55-year Reanalysis	Kobayashi et al. (2015)	1985-2018	L60, 0.2 hPa
CTM+MERRA2	Modern-Era Retrospective analysis for Research and Applications	Gelaro et al. (2017)	1985-2018	L72, 0.01 hPa
ACE-FTS	Atmospheric Chemistry Experiment Fourier Transform Spectrometer	Bernath et al. (2021)	2005-present	L42, 150 km

Table 1. Overview of the models and satellite measurements used in this study.

Station name	Reference	Location (lat and lon)	Altitude	strato DOFS
Lauder	Zhou et al. (2019)	45.4°S and 169.68°E	370 m	2
Wollongong	Griffith et al. (2012)	34.45°S and 150.88°E	30 m	2
Izaña	García et al. (2021)	28.30°N and 16.48°E	2367 m	1.5
Jungfraujoch	Zander et al. (2008)	46.55°N and 7.98°E	3580 m	1.1

Table 2. Overview of FTIR stations considered in this study.

2.1 Ground-based FTIR Observations

We use ground-based measurements of stratospheric N_2O columns obtained at four stations that are part of NDACC: Lauder (New Zealand, 45°S), Wollongong (Australia, 34°S), Izaña (Spain, 28°N) and Jungfraujoch (Switzerland, 46°N) (Zhou et al., 2019). The solar absorption spectra under clear-sky conditions with the ground-based FTIR measurements taken under the auspices of the NDACC allow the acquisition of long-term consistent data sets. The stations have been chosen at the mid-latitudes and subtropics where the observed BDC changes are the largest (e.g., Strahan et al., 2020).

At Jungfraujoch, measurements have been obtained from two spectrometers: an instrument developed at the University of Liège (1984-2008), and a Bruker IFS 120HR (early 1990's-present) (Zander et al., 2008; Prignon et al., 2019). In this study, we use the spectra taken by the Bruker spectrometer to investigate the most recent period. Ground-based measurements of N_2O profiles at Lauder started in 2001 with a Bruker 120HR spectrometer, replaced in 2018 (with 6 months overlap) by a Bruker 125HR (Strong et al., 2008; Zhou et al., 2019). The Lauder station is particularly relevant as is the only FTIR site of NDACC located in the SH mid-latitudes. The Wollongong station has provided data for the SH subtropics since 1996. Solar spectra were measured with a Bomem instrument until 2007, which was then replaced by a Bruker 125HR (Griffith et al., 2012). N_2O profiles are also measured at the Izaña Observatory since 1999. This high-altitude station is characterized by excellent conditions for FTIR spectroscopy, with clear sky conditions for most of the year. Observations started using a Bruker 120M spectrometer and continued, since 2005, with a Bruker 125HR (García et al., 2021). The retrieval code for the N_2O profiles is the SFIT-v4 (v0.9.4.4) for the Jungfraujoch, Lauder and Wollongong stations, and PROFITT9 for the Izaña station (Zhou et al., 2019).

We consider stratospheric N_2O columns between 12 and 40 km of altitute because the instruments at all stations are the most sensitive to the measured N_2O profiles over this stratospheric region (not shown). The degrees of freedom for signal (DOFS), which quantify the vertical resolution of the measurement (Rodgers, 2000), vary largely between the stations. For N_2O, the stratospheric DOFS between 12 and 40 km of the instruments in the SH are approximately 2, allowing the separation of two layers within the stratosphere. On the other hand, the stratospheric DOFS of the instruments in the NH are around 1.5 for Izaña, and 1 for Jungfraujoch, limiting the analysis to one stratospheric layer between 12 and 40 km. Thus, in order to perform a fair comparison, we compute one stratospheric N_2O column between 12 and 40 km for all stations. In order to take into account the limited sensitivity of the FTIR measurements, we smooth the ACE-FTS data and the model output on the FTIR vertical grid using the FTIR averaging kernels as described in Langerock et al. (2015).

2.2 Spaceborne Measurements - ACE-FTS

ACE-FTS, onboard the SCISAT Canadian satellite, was launched in August 2003 on a high inclination (74°) low earth orbit (650 km) and is still in operation in 2022 (Bernath et al., 2005; Bernath, 2017). The ACE-FTS instrument measures the infrared absorptions from solar occultations between 2.2 and 13.3 μm with a spectral resolution of 0.02 cm^{-1}. This allows the retrieval of vertically resolved mixing ratio profiles for 44 molecules and 24 isotopologues from each measurement (Bernath et al., 2020).

In this study, we use version 4.1 of the ACE-FTS data. It differs from previous versions by the significantly better retrievals at low altitudes and led to substantially improved trends compared to the earlier version 3.5 (Bernath et al., 2021). For N_2O, previous comparisons of v3.6 with independent satellite instruments showed a good agreement below 35 km (within 10%) and larger biases above that level (within 20%, Sheese et al., 2017). In our study, N_2O profiles are filtered for outliers using the method described in Sheese et al. (2017) and are then vertically regridded to a constant pressure vertical grid using a mass-conservative scheme (Bader et al., 2017). For trend analysis, profiles are monthly averaged on latitude bins with 5°spacing from pole to pole.

In order to compare the trend analysis of model simulations with those obtained by ACE-FTS, the model datasets are first re-sampled from their native temporal and spatial grids (model space) to match those of ACE-FTS (observational space). This is important in particular due to the low sampling of ACE-FTS - only 30 daily profiles due to the solar occultation method. The re-sampling is done by finding model output adjacent in time to each ACE-FTS profile (BASCOE and WACCM datasets used in this study have, respectively, 6 hourly and daily output) and then by linearly interpolating the model values in time and space at the profile geolocation. The re-sampled model datasets are then averaged over a month as done with ACE-FTS.

2.3 BASCOE CTM and Driving Reanalyses

In this study, we use the BASCOE CTM driven by four dynamical reanalyses: the European Centre for Medium-Range Weather Forecast Interim reanalysis (ERAI, Dee et al., 2011), and its newer version ERA5 (Hersbach et al., 2020), the Modern-Era Retrospective analysis for Research and Applications version 2 (MERRA2, Gelaro et al., 2017), and the Japanese 55-year Reanalysis (JRA55, Kobayashi et al., 2015). In the following, we provide a brief overview of the BASCOE CTM and the ERAI, MERRA2 and JRA55 reanalyses, as more detailed information can be found in such companion studies: Chabrillat et al. (2018); Prignon et al. (2019, 2021) and M2020. Since ERA5 is not detailed in these publications, we provide a more detailed description.

The BASCOE CTM is built on a kinematic transport module (that takes as input the surface pressure and the horizontal winds) with a flux-form semi-Lagrangian (FFSL) advection scheme (Lin & Rood, 1996). The FFSL scheme is run on a common horizontal grid of 2°x2.5°for all the reanalyses, while the vertical grid depends on the input reanalysis. The chemical scheme explicitly solves for stratospheric chemistry, and includes 65 chemical species and 243 reactions (Prignon et al., 2019). ERAI and JRA55 have 60 levels up to 0.1 hPa, MERRA2 has 72 levels up to 0.01 hPa. The model setup, as well as the boundary conditions (including those for N_2O), are the ones used in Prignon et al. (2019), M2020 and Prignon et al. (2021). Readers are directed towards Chabrillat et al. (2018) for a detailed description of the BASCOE CTM and its driving by the ERAI, JRA55 and MERRA2 reanalyses.

The ERA5 reanalysis is the fifth generation of reanalysis produced by the ECMWF and covers the 1979-present period, with a programmed extension back to 1950 (Hersbach et al., 2020). The horizontal resolution is 31 km, with hourly output frequency, and the vertical grid ranges from the surface to 0.01 hPa with 137 levels and with 300-600 m vertical spacing in the troposphere and stratosphere, which increases to 1-3 km above 30 km. ERA5 suffers from a cold bias in the lower stratosphere from 2000 to 2006. For this reason, a new analysis (ERA5.1) has been produced for that period to correct for that bias (Simmons et al., 2020). In this study, the BASCOE CTM was driven by ERA5.1 for the 2000-2006 period. For computational reasons, the vertical resolution is reduced to 86 levels from the original 137 keeping the original vertical spacing in the stratosphere, and we used 6-hourly (0000, 0600, 1200, 1800 UTC) data. As done for the other reanalyses, the ERA5 data on the fine 31-km grid were truncated at wavenumber 47 to avoid aliasing on the target 2.5°x2°horizontal grid (Chabrillat et al., 2018).

In order to further investigate the contribution of transport in ERA5, we performed two sensitivity tests with the BASCOE CTM driven by that reanalysis. To isolate the contribution of transport, the first sensitivity test consists of a fixed N_2O run, i.e., a BASCOE CTM simulation where N_2O does not increase over time. We accomplished that by performing a BASCOE CTM run exactly as the ERA5 simulation but keeping the N_2O volume mixing ratios at the surface fixed to their values at the beginning of the simulation (cst-N_2O). Any N_2O trend for the cst-N_2O simulation is therefore due only to the effect of transport. The second sensitivity test is a perpetual year simulation that is complementary to cst-N_2O, and consists of an experiment where the transport does not change over time (cst-dyn). In order to include a complete Quasi Biennial Oscillation cycle (QBO, Baldwin et al., 2001), we used the years 2006 and 2007 from ERA5.1 and ERA5, respectively. Those years are unusual (but convenient) because the QBO lasted exactly 24 months (see the zonal wind data at Singapore `https://www.geo.fu-berlin.de/met/ag/strat/produkte/qbo/singapore.dat`). We used the dynamics of the year 2006 to simulate even years and from the year 2007 for odd years. All the N_2O changes simulated by cst-dyn are due to its constant increase at the surface.

2.4 WACCM

In this study, we use two versions of WACCM: version 4 (Marsh et al., 2013; Garcia et al., 2017) and version 6 (Gettelman et al., 2019). WACCM version 4 (WACCM4) is the atmospheric component of the Community Earth System Model version 1.2.2 (CESM, Hurrell et al., 2013), which has been developed by the U.S. National Center of Atmospheric Research. It is the extended (whole atmosphere) version of the Community Atmosphere Model version 4 (CAM4, Neale et al., 2013). WACCM4 has a longitude-latitude grid of 2.5°x1.9°and 66 vertical levels from the surface to about 140 km altitude, with 1.1-1.75 km vertical spacing in the stratosphere. The physics of WACCM4 is the same as CAM4 and the dynamical core is a finite volume with a horizontal discretization based on a conservative flux-form semi Lagrangian (FFSL) scheme (Lin, 2004). WACCM4 is not able to internally generate the QBO; thus, it is nudged towards observations of stratospheric winds (Matthes et al., 2010). In this study, we use the WACCM4 version included within the SPARC (Stratosphere-troposphere Processes And their Role in Climate) Chemistry-Climate Model Intercomparison phase 1 (CCMI-1, Morgenstern et al., 2017). In particular, we use the REFC1 experiments (WACCM-REFC1), which consist of simulations of the recent past (1960-2018) using state-of-the-art historical forcings and observed sea-surface temperatures (Morgenstern et al., 2017). For N_2O , the boundary conditions are prescribed using the forcing recommended by the CCMI (Eyring et al., 2013). Compared to the default WACCM4 version, WACCM-REFC1 includes important modifications of the treatment of heterogeneous chemistry and of the gravity waves parameterization, which ultimately improve the simulation of ozone in the Southern Hemisphere (Garcia et al., 2017). In this study, we use three realizations of the WACCM-REFC1 configuration for the 1985-2018 period.

Version 6 of WACCM (WACCM6) is the extension to the whole atmosphere of version 6 of CAM that is part of version 2 of CESM (Danabasoglu et al., 2020). The default horizontal resolution of WACCM6 is 0.9°x1.25°latitude-longitude, with 70 levels in the vertical from the ground to around 140 km, with vertical resolution similar to WACCM4. The transition from WACCM4 to WACCM6 involved several changes in the physics and chemistry that are described in Gettelman et al. (2019). WACCM6 is part of the Coupled Model Intercomparison Project Phase 6 (CMIP6, Eyring et al., 2016), and is used in the CCMI-2022 activity (i.e., the successor of CCMI-1, Plummer et al., 2021). Within CCMI-2022, we use the REFD1 WACCM6 experiments (WACCM-REFD1), i.e., a suite of hindcast experiments for the recent past (1960-2018) used to compare with observations. The REFD1 experiments use the databases for historical forcings and observed sea surface temperatures developed for the CMIP6. The N_2O emissions are specified following the CMPI6 recommendation for historical simulations, i.e., following Meinshausen et al. (2020). Although WACCM6 can internally produce the QBO, the REFD1 experiments require a nudged QBO towards observed winds to ensure synchronization with historical variability. In this study, we use one realization of the WACCM-REFD1 experiments for the 1985-2018 period.

2.5 TEM Diagnostics

For stratospheric tracers, the TEM diagnostics (Andrews et al., 1987) allows separating the impact of transport and chemistry on the zonal mean local rate of change of a tracer with mixing ratio χ:

$$\overline{\chi}_t = -v^*\overline{\chi}_y - w^*\overline{\chi}_z + e^{z/H}\nabla \cdot \mathbf{M} + \overline{S} + \overline{\epsilon}, \tag{1}$$

where χ represents N_2O, $\mathbf{M} = -e^{-z/H}(\overline{v'\chi'} - \overline{v'\theta'}\overline{\chi}_z/\bar{\theta}_z, \overline{w'\chi'} + \overline{v'\theta'}\overline{\chi}_y/\bar{\theta}_z)$ is the eddy flux vector, and (v^*, w^*) are the meridional and vertical components of the residual circulation, respectively. Overbars denote zonal means and prime quantities indicate deviations from it, while subscripts indicate partial derivatives. $H = 7$ km is the scale height, and $z \equiv -Hlog_e(p/p_s)$ is the log-pressure altitude, with the surface pressure $p_s = 10^5$ Pa. The S term is the net rate of change due to chemistry, defined as the difference between the production ($\bar{P}$) and loss ($\bar{L}$) rates $\bar{S} = \bar{P} - \bar{L}$. The $\overline{\epsilon}$ contribution represents the residual of the budget, i.e., the difference between the actual rate of change of $\overline{\chi}$ and the sum of the transport and chemistry terms on the right-side hand of Eq. 1.

The transport terms in Eq. 1 can be grouped as follows:

$$\overline{\chi}_t = ADV + MIX + \overline{S} + \overline{\epsilon}, \tag{2}$$

where $ADV = (-v^*\overline{\chi}_y - w^*\overline{\chi}_z)$ and $MIX = e^{z/H}\nabla \cdot \mathbf{M}$ represent the contribution of the residual circulation and of the resolved mixing, respectively. We refer to M2020 for a more detailed description of the TEM framework applied to the N_2O mixing ratios in the stratosphere and for a comprehensive discussion of the contribution of each term to the N_2O budget.

2.6 Derivation of Trends with the Dynamical Linear Modelling Tool

In this study, we investigate decadal trends using the Dynamical Linear Modeling regression tool (DLM, Alsing, 2019). DLM is based on Bayesian inference and provides a number of possible models to analyze time series. Each model is characterized by some unknown parameters, and the DLM computes the posterior probability distribution of those parameters using a combination of Kalman filtering and Markov chain Monte Carlo method.

For a given atmospheric time-series y_t, a generic DLM model is composed of four components: a linear background trend, a seasonal cycle with 12- and 6-months periods, forcing terms decribed by a number of regressor variables and an auto-regressive component:

$$
\begin{aligned}
y_t \quad = \quad & \beta_{1,t} z_{1,t} + \beta_{2,t} z_{2,t} ... + \beta_{n,t} z_{n,t} \\
& + \beta^{12}_{1,t} \sin(2\pi t/12) + \beta^{12}_{2,t} \cos(2\pi t/12) \\
& + \beta^{6}_{1,t} \sin(2\pi t/6) + \beta^{6}_{2,t} \cos(2\pi t/6) \\
& + \mu_t \\
& + z^{AR}_t \\
& + \epsilon_t .
\end{aligned} \tag{3}
$$

In Eq. 3, the terms $\beta_{i,t} z_{i,t}$ represent the contribution to y_t from the regressors, where $z_{i,t}$ is the corresponding time-series for each regressor. The 6- and 12-months seasonal cycles are modeled respectively by $\beta^{6}_{1,t} \sin(2\pi t/6) + \beta^{6}_{2,t} \cos(2\pi t/6)$ and $\beta^{12}_{1,t} \sin(2\pi t/12) + \beta^{12}_{2,t} \cos(2\pi t/12)$. The μ_t term denotes the linear fit term, and z^{AR}_t the auto-regressive term, defined similarly to the Cochrane-Orcutt correction (Kyrölä et al., 2013), and ϵ_t is the uncertainty.

Contrarily to a multi-linear regression (MLR) model, the background linear fit μ_t and the amplitudes of the seasonal cycles $\beta^{6,12}_{i,t}$ in DLM can vary with time (i.e., they are non-parametric). Their degrees of time-dependence are the unknown model parameters and are initially set by the user and inferred from the data during the model run. Furthermore, the auto-regressive process in the DLM is computed within the model run together with the other parameters, not as a post-run correction as done in the MLR, and its uncertainties are carefully taken into account within the error propagation. In addition, the standard DLM implementation has time-varying (heteroscedastic) uncertainty distribution, when time-varying uncertainties are available. DLM was recently used to investigate stratospheric ozone trends in observations and models (Ball et al., 2017, 2018). A more detailed description of the DLM models and their implementation can be found in Laine et al. (2014). For a more comprehensive review of time-series analysis using DLM, refer to Durbin and Koopman (2012).

As regressor variables, we used the 30 cm radio flux as a solar proxy (de Wit et al., 2014), an index for the El-Nino Southern Oscillation (Wolter & Timlin, 2011) from the National Oceanic and Atmospheric Administration (`http://www.esrl.noaa.gov/psd/enso/mei/`), and two indices for the QBO at 30 and 50 hPa from the Freie Universität Berlin (`http://www.geo.fu-berlin.de/en/met/ag/strat/produkte/qbo/index.html`). We fed the DLM model with monthly data, running 3000 samples where the first 1000 were considered as a warmup and discarded. We also tried 10000 realizations and 3000 as warmup with very similar results (not shown). We performed several sensitivity tests to determine the appropriate values of the initial model parameters, i.e., the degree of time-dependence of the linear trend and seasonal cycles, in order to allow a reasonable time-dependence without being unrealistic. The different combinations of these values did not provide significant differences, so we kept the recommended values.

The linear trends are computed from the distribution of the fit samples μ_t as the difference between the end and start dates of the considered period (delta= $\mu_t[end] - \mu_t[start]$), weighted by the number of the years. From the resulting delta distribution, the uncertainties associated with the trend are computed as the percentage of its positive (negative) values. This percentage can be interpreted as the posterior probability that the trend is positive (negative) between the considered dates. In this way, we do not make any assumption on the shape of the distribution of the trends.

3 Stratospheric N_2O Columns and their Trends

Figure 1 shows the linear fits of the monthly stratospheric N_2O columns (12-40 km) at the four FTIR stations, together with the initial N_2O columns from the observations and the ERA5 simulation. In this analysis, we do not apply the FTIR time sampling to the model output because sensitivity tests using WACCM-REFD1 at each station showed no significant impact of the FTIR time sampling on the recovered trends of the N_2O columns (not shown). The stratospheric N_2O columns computed between 12 and 40 km of altitude are highly sensitive to the N_2O increase in the lower stratosphere, which is mainly the result of the continuous growth in the troposphere (Tian et al., 2020) and can also be impacted by structural changes of the atmosphere (e.g., the global rise of the tropopause, Xian & Homeyer, 2019). Consequently, all datasets exhibit an increase in the stratospheric N_2O columns over the last two decades.

Above Lauder, the linear fit of the stratospheric N_2O columns from the ERA5 simulation is in agreement with the observations, similarly to JRA55 and ERAI. WACCM-REFD1 underestimates the stratospheric N_2O columns compared to the observations by around 10%, and performs worse than its earlier version WACCM-REFC1, which differs from the observations by only 5%. At Wollongong, the slope of the linear fit of the N_2O columns measured by the FTIR, and to a lesser extent by ACE-FTS, is steeper before 2005 compared to the following period. This change of gradient is not visible in any of the model simulations. On the contrary, some of the models show a slower increase before 2005, followed by a more rapid increase (e.g., the ERA5 simulation). Contrarily to Lauder, the WACCM-REFD1 simulation delivers more realistic stratospheric N_2O columns compared to its previous version WACCM-REFC1.

Above Izaña, all the models underestimate the stratospheric N_2O columns with respect to the FTIR observations, with the largest difference reaching 14% for MERRA2. Concerning ACE-FTS, the bias with FTIR measurements is around 8%, which is qualitatively consistent with the results of Strong et al. (2008), even though they used v2.2 of ACE-FTS. However, García et al. (2021) showed good agreement above Izaña for tropospheric N_2O abundances and total N_2O columns obtained from independent measurements. The difference between the stratospheric N_2O columns measured by FTIR and ACE-FTS could be explained by the poor coverage of ACE-FTS over the tropical and subtropical regions. Since the ACE-FTS measurements represent a latitude band, the observed N_2O results biased towards the values measured at higher latitudes, where more occultations are available (Kolonjari et al., 2018). Since the N_2O abundances decrease poleward (Jin et al., 2009), this could explain the low bias in the stratospheric N_2O columns measured by ACE-FTS compared to those obtained from FTIR.

Above Jungfraujoch, there is the largest spread in the linear fits of the stratospheric N_2O columns, with the largest differences reaching around 25% between ACE-FTS and WACCM-REFD1. Prignon et al. (2019) compared lower stratospheric columns of chlorodifluoromethane (HCFC-22) between an earlier WACCM version and FTIR measurements, and showed that WACCM consistently underestimates the HCFC-22 columns compared to the FTIR measurements. Since both N_2O and HCFC-22 (which has an atmospheric lifetime of 12 years, Prignon et al., 2019) are produced at the surface and transported into the stratosphere, this underestimation in WACCM could indicate a shortcoming in simulating the accumulation of long-lived tracers in the stratosphere above the northern mid-latitudes. Indeed, Angelbratt et al. (2011) already highlighted that the stratospheric transport has a large impact on the N_2O columns above Jungfraujoch compared to stations at higher latitudes. Regarding the observational datasets, there is a considerable disagreement between the FTIR instrument and ACE-FTS before 2012, showing increasing and decreasing N_2O columns, respectively. This is in contrast with the remarkably good agreement in the SH between the two datasets. This difference between the stratospheric N_2O columns in ACE-FTS and FTIR measurements will be further addressed in Sect. 4.

In the Tropics and above the lower stratospheric mid-latitudes, the N_2O abundances are inversely proportional to the mean AoA (Andrews et al., 2001; Strahan et al., 2011; Galytska et al., 2019). The stratospheric N_2O columns at mid-latitudes considered here

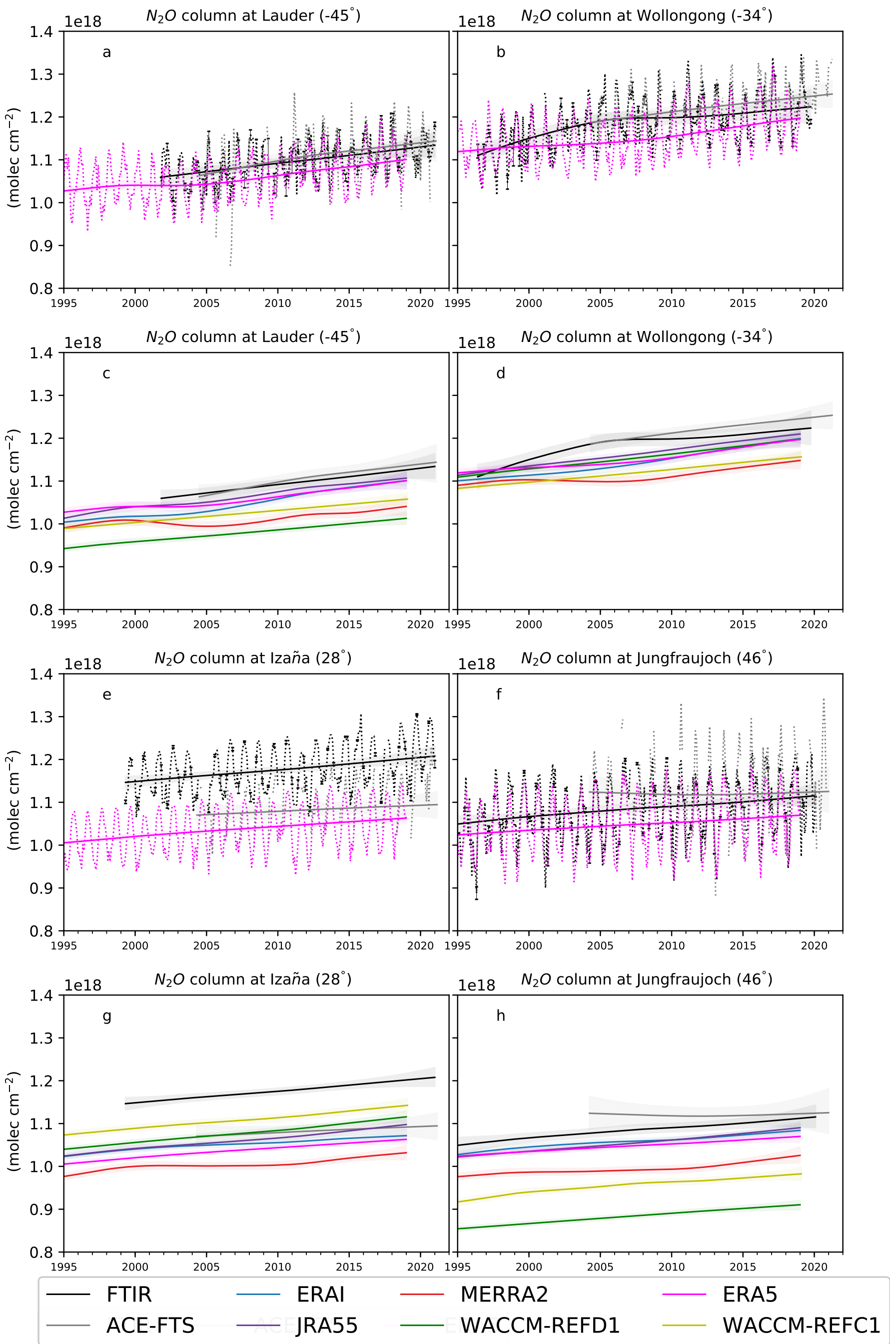

Figure 1. Time-series of stratospheric N_2O columns (12-40 km) from observations and models at four stations. Continuous lines show the linear fit obtained by the DLM regression, dashed lines depict the N_2O column data. The color code is shown in the legend. The vertical error bars in panels a,b,e,f represent the standard error of the monthly mean. Panels a,b show Lauder, panels b,d show Wollongong, panels e,g show Izaña and panels f,h show Jungfraujoch. Panels a,b,e,f: DLM fits and data for FTIR and ACE-FTS measurements and the BASCOE simulation driven by ERA5. Panels c,d,g,h: DLM fits for all the datasets considered. The model and satellite data are interpolated to the longitude and latitude of the station, and vertically regridded to match the retrieval layering schemes. After the regridding, the data were smoothed using the FTIR averaging kernels. The colored shadings represent the uncertainties from the 2.5 and 97.5 percentiles of the distributions from the DLM.

are highly sensitive to the N_2O abundances in the lower stratosphere, hence the inverse relationship also holds for the stratospheric N_2O columns above the mid-latitudes. Thus, the lower stratospheric N_2O columns in MERRA2 compared to the other datasets across the stations are consistent with the older mean AoA throughout the stratosphere found using MERRA2 by Chabrillat et al. (2018). The N_2O distribution in the stratosphere is opposite also to the total inorganic fluorine F_y. N_2O is emitted in the troposphere while F_y is produced in the stratosphere, and, as a consequence of the poleward transport of the BDC, N_2O is removed and F_y is increased in the stratospheric mid-latitudes. In the light of this relationship between N_2O and F_y, the underestimated N_2O columns above Lauder and Jungfraujoch in MERRA2 are consistent with larger stratospheric F_y columns in MERRA2 compared to the other reanalyses above those stations (Prignon et al., 2021).

Figure 2 shows distributions of the trend of the stratospheric N_2O columns obtained from the respective linear fits over the common period 2005-2018. The N_2O trends at the surface have already been compared for a number of FTIR stations (including Lauder, Wollongong and Izaña) against observations from flask samples, showing an excellent agreement (Zhou et al., 2019).

Above Lauder, the N_2O trends obtained with ERA5 and JRA55 are in good agreement with the FTIR measurements, but are underestimated in WACCM-REFD1 (around 25%) with no particular improvement with respect to WACCM-REFC1. The ERAI simulation delivers the largest N_2O trends, with more than 30% difference with respect to the FTIR measurements. At Wollongong, the N_2O trend obtained with the FTIR measurements is the smallest because the N_2O increase above that station is smoother compared to the other datasets. Interestingly, the N_2O trend simulated by WACCM-REFD1 is the closest to the trend obtained from the FTIR observations, while the trend obtained with ERA5 is almost twice as large. As for Lauder, the N_2O trends obtained from ERAI are the largest at this station. Above Izaña, WACCM-REFD1 agrees remarkably well with the FTIR (difference around 3%), while the trend from ERA5 lies between the trends measured from FTIR and ACE-FTS, with around 20% difference compared to FTIR. Above Jungfraujoch, the trend in the N_2O columns from WACCM-REFD1 agrees with the trend from the FTIR within 10% difference and is similar to what is obtained with ERA5. The largest trends are obtained with MERRA2 and JRA55, reaching 13% and 30% difference compared to the FTIR, respectively. The decreasing N_2O stratospheric column in ACE-FTS before 2012 results in a near-zero trend, which is in contrast with the trends obtained by the other datasets, which approximately range from 2 to 3×10^{15} molec cm^{-2} year $^{-1}$.

Considering decadal changes, the observations and the ERA5 and ERAI simulations show larger trends of the stratospheric N_2O columns in the SH than in the NH, especially at mid-latitudes (respectively Lauder and Jungfraujoch). WACCM-REFD1 also shows this hemispheric difference at mid-latitudes, which is a clear improvement with respect to WACCM-REFC1. Those asymmetries are consistent with the results of Strahan et al. (2020), who found significantly negative mean AoA trends in the SH compared to the NH using HCl and HNO_3 measured at several ground-based FTIR stations. In addition, the hemispheric differences of the N_2O trends are also consistent with the results of Prignon et al. (2021), who found larger and more significant F_y trends from FTIR above Jungfraujoch than above Lauder.

We conclude the section by providing a short description of the limits of using stratospheric columns of N_2O from FTIR measurements. As mentioned earlier, the stratospheric N_2O columns between 12 and 40 km are primarily influenced by the steady increase in the lowermost stratosphere below 15 km. The DOFS of the FTIR instrument at Jungfraujoch for the stratosphere (12-40 km) is close to 1.1. Thus, the FTIR measurements at that station cannot resolve more than one partial column between 12 and 40 km, which can hinder the detection of N_2O trends in the middle and upper stratosphere (i.e., above 30 km) because of the influence of the increase in the lowermost stratosphere. Indeed,

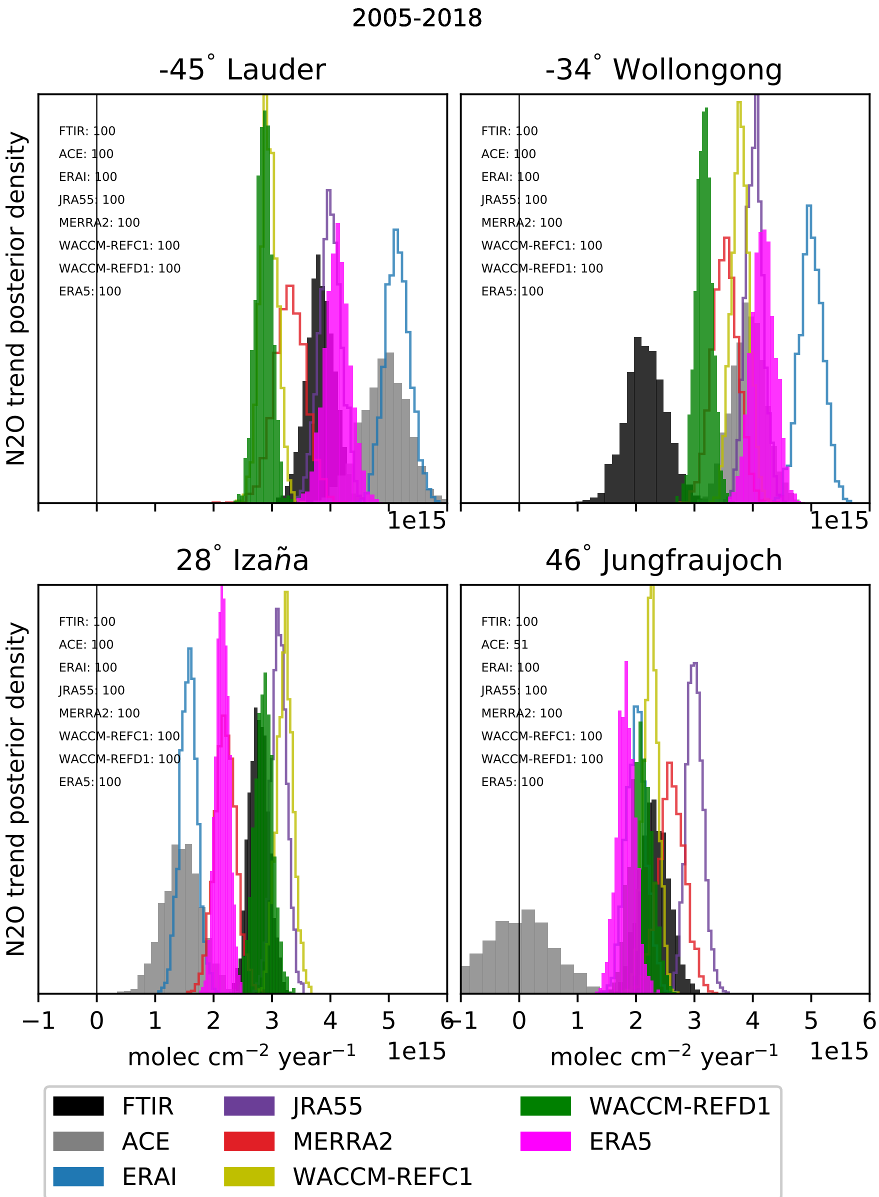

Figure 2. Posterior probability of positive changes of the DLM linear trend of the stratospheric N_2O columns (12-40 km) for the four FTIR stations (2005-2018). The color code is shown in the legend. For reference, the N_2O trend in the troposphere (5.5-10.5 km) is approximated from the data in Bernath et al. (2020) as 4.3e15 molec cm^{-2} year^{-1}.

it was shown that stratospheric N_2O trends over the last decades, obtained both from satellite measurements and model simulations, do not consist of just a global increase, but largely depend on latitude and height (e.g., Froidevaux et al., 2019). Therefore, we will consider latitudinal- and vertical-dependent trends of N_2O mixing ratios in the following section.

4 Global N_2O Linear Trends

4.1 Trends in the ACE-FTS Observational Space

Figure 3 shows latitude-vertical cross sections of the linear trends of the N_2O mixing ratios for the various datasets, over the 2005-2018 period. In order to reduce the sampling bias, the model datasets are sampled in space and time as the ACE-FTS measurements before the computation of the trends. We use the ACE-FTS measurements as a reference, because they encompass this period with global coverage and good stability (Bernath et al., 2020, 2021).

In the upper stratosphere above 10 hPa, the N_2O trends from ACE-FTS are positive, with larger trends in the NH that are found significant at lower levels than in the SH. The ERAI-driven simulation qualitatively reproduces these patterns in the upper stratosphere, while the other model datasets differ from ACE-FTS, especially ERA5. A common feature among all datasets is an increase in N_2O above the Equator in the upper stratosphere, around 5 hPa. At those altitudes of the tropical pipe, the upward transport of N_2O by the residual circulation reaches its maximum (see M2020).

In the mid-lower stratosphere below 20 hPa, ACE-FTS shows a clear hemispherical asymmetry (meridional dipole) in the N_2O trends, with significantly negative values in the NH and significantly positive in the SH. Above the location of Jungfraujoch (the most northern vertical green line), the negative N_2O trend detected by ACE-FTS in the mid-lower stratosphere is responsible for the disagreement with the FTIR observations discussed in the previous section, as the layer of the stratospheric N_2O column encompasses regions of both positive (lowermost and upper stratosphere) and negative (mid-lower stratosphere) N_2O trends. The meridional dipole is significant also over a shorter period (2005-2012, not shown) and corroborates a number of previous findings over that period using satellite measurements of HCl (Mahieu et al., 2014) and mean AoA derived from space-borne measurements of SF_6 (Haenel et al., 2015). In regions where the N_2O abundances are larger than 100 ppbv, i.e., approximately below 10 hPa, the N_2O linear trends are opposite to those obtained with its product NO_2, because the two tracers are correlated by an inverse linear relationship (Plumb & Ko, 1992). Below 20 hPa, the N_2O meridional dipole from ACE-FTS is consistent with the pattern of the decadal trends of NO_2 obtained from independent satellite measurements (Galytska et al., 2019; Dubé et al., 2020).

The meridional dipole in the N_2O trends derived from ACE-FTS is generally reproduced by the CTM simulations, with ERAI and ERA5 delivering trends that are most similar to the satellite measurements. Prignon et al. (2021) used the same simulations as the present study to investigate global stratospheric trends of total inorganic fluorine F_y. The dipoles obtained here in the N_2O trends from the ECMWF reanalyses are consistent with the opposite trends of F_y for almost the same period (Prignon et al., 2021). For WACCM, the strength of the N_2O meridional dipole is globally reduced compared to ACE-FTS, with weaker and not significant negative N_2O trends over the NH. However, WACCM-REFD1 performs better than WACCM-REFC1 over the SH, with stronger and significant positive N_2O trends that reach 30 hPa, similarly to those obtained with ACE-FTS in the same region. This improvement is possibly related to the changes in the parametrization of the gravity waves (i.e., small-scale tropospheric waves that drive the BDC) in WACCM version 6 compared to version 4 that followed the increase of its

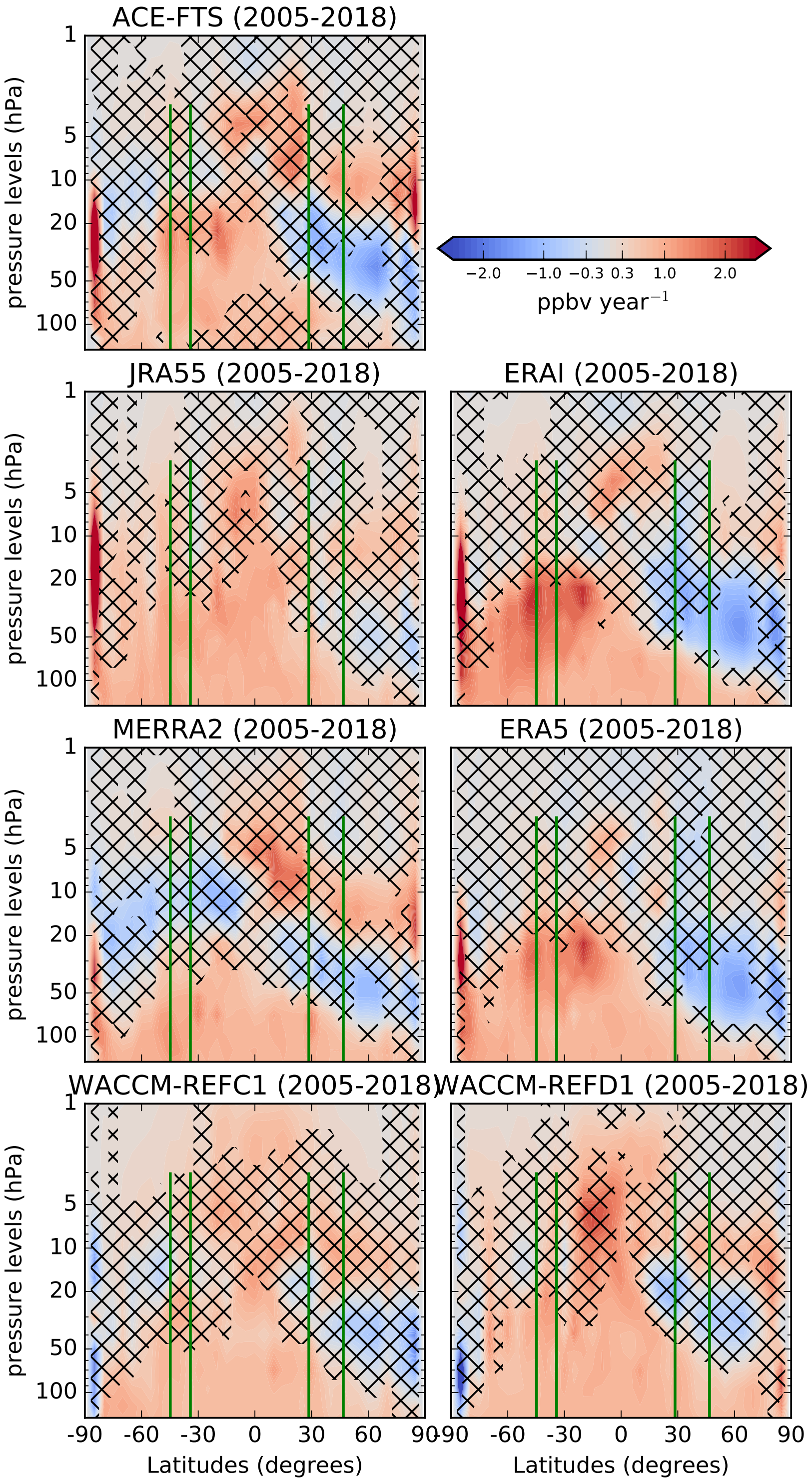

Figure 3. Latitude-pressure cross-sections of N_2O linear trends (pptv year^{-1}) obtained from the DLM (2005-2018). The N_2O simulated by the model is interpolated to the location and timing of the observations, see text for details. The black crosses indicate grid-points where the probability of positive/negative N_2O changes is smaller than 95%. The green vertical lines identify the position of the FTIR stations together with their vertical coverage.

horizontal resolution (Gettelman et al., 2019). This new parametrization results in a good agreement between the gravity waves simulated by WACCM and the observations in the Tropics (Alexander et al., 2021). For tracers, the favorable effect of adjusting the parameterization of the gravity waves in WACCM was shown for ozone in the extratropical SH by Mills et al. (2017). Over the same region, the improved N_2O trends in WACCM-REFD1 compared to WACCM-REFC1 could be attributed to the new parameterization of the gravity waves. This beneficial impact would be consistent with the results of M2020, which showed similar improvements in the N_2O climatologies between two WACCM versions differing by the parametrization of gravity waves over the SH.

In the lowermost stratosphere (pressure greater than 100 hPa), all models and ACE-FTS show positive N_2O trends, resulting from the constant increase in the troposphere. However, the N_2O increase in the lowermost stratosphere (below 70 hPa) over the Tropics and the NH is not significant in ACE-FTS, contrary to the model simulations. This difference could be related to the stronger trends in the tropopause rise in the models: around 50 m/decade in CCMs (including WACCM) and ERA5 (Pisoft et al., 2021; Darrag et al., 2022) compared to the observations (around 35 m/decade, Darrag et al., 2022) when using the tropopause definiton from the World Meteorological Organization.

4.2 Trends in the Model Space

Figure 4 shows the N_2O trends as in Fig. 3, but without applying the ACE-FTS spatial and temporal sampling. A comparison between each model simulation in the observation and model space (respectively Fig. 3 and Fig. 4) reveals large differences in the N_2O decadal trends. Generally, the sampling of the ACE-FTS observations enhances the trends simulated by the models, both in the negative and positive directions. For the ERA5 simulation, the significantly negative trend in the NH in observational space becomes insignificant in model space. In addition, one notes immediately that the N_2O trends in the WACCM simulations change sign, with negative trends in the NH in the observational space becoming weakly positive in model space. In particular for WACCM-REFD1, the N_2O trends over the northern mid-latitudes in the mid-low stratosphere substantially increase from -0.5 ppbv year^{-1} in observational space to 0.3 ppbv year^{-1} in native model space. However, this difference is not significant because neither of the N_2O trends above that region is statistically significant with 95% probability.

For satellite measurements, the impact of the sampling in the detection of trends in long-lived species (including N_2O) has been evaluated in Millán et al. (2016). They concluded that large errors may arise in the detected trends for coarse and non-uniform sampling obtained with occultation instruments (such as ACE-FTS), and that long time scales are required for a robust trend detection from these datasets. Such errors also occur in the models when they are sampled in space and time as the observations. In particular, within the DLM, the non-uniform time sampling of ACE-FTS considerably increases the standard deviation of the error in the N_2O time series, which is zero for regular time sampling. This difference plays a role when deriving trends over these relatively short (decadal) time scales. For example, the non-uniform ACE-FTS sampling applied to the ERA5 output results in negative N_2O trends that are 4 times stronger compared to the native grid above the northern mid-latitudes between 50 and 70 hPa. For WACCM, the issue of downsampling was also raised by Garcia et al. (2011) when comparing mean AoA trends obtained from balloon-borne observations and simulated by the model. Garcia et al. (2011) showed that sampling the model as the observations would deliver positive and non-significant mean AoA trends, similarly to the observations. We find consistent results with the WACCM simulations: sampling the WACCM output as the observations drives the N_2O trends towards the observed values. In addition, the non-significant negative N_2O trends simulated by WACCM are compatible with the non-significant positive mean AoA trends found by Garcia et al. (2011) when downsampling WACCM at

Figure 4. As in Figure 3, but in the model space.

5/2481/2012/ doi: 10.5194/amt-5-2481-2012

Haenel, F. J., Stiller, G. P., von Clarmann, T., Funke, B., Eckert, E., Glatthor, N., . . . Reddmann, T. (2015). Reassessment of MIPAS age of air trends and variability. Atmospheric Chemistry and Physics, 15(22), 13161{13176. Retrieved from https://acp.copernicus.org/articles/15/13161/2015/ doi: 10.5194/acp-15-13161-2015

Hall, T. M., & Plumb, R. A. (1994). Age as a diagnostic of stratospheric transport. Journal of Geophysical Research: Atmospheres, 99(D1), 1059{1070.

Han, Y., Tian, W., Chipper eld, M. P., Zhang, J., Wang, F., Sang, W., . . . Tian, H. (2019). Attribution of the Hemispheric Asymmetries in Trends of Stratospheric Trace Gases Inferred From Microwave Limb Sounder (MLS) Measurements. Journal of Geophysical Research: Atmospheres, 124(12), 6283-6293. Retrieved from https://agupubs.onlinelibrary.wiley.com/doi/abs/10.1029/2018JD029723 doi: https://doi.org/10.1029/2018JD029723

Hardiman, S. C., Butchart, N., & Calvo, N. (2014). The morphology of the Brewer{Dobson circulation and its response to climate change in CMIP5 simulations. Quarterly Journal of the Royal Meteorological Society, 140(683), 1958{1965.

Hardiman, S. C., Lin, P., Scaife, A. A., Dunstone, N. J., & Ren, H.-L. (2017). The in uence of dynamical variability on the observed Brewer{Dobson circulation trend. Geophysical Research Letters, 44(6), 2885{2892.

Harrison, J. J., Chipper eld, M. P., Boone, C. D., Dhomse, S. S., Bernath, P. F., Froidevaux, L., . . . Russell III, J. (2016). Satellite observations of stratospheric hydrogen uoride and comparisons with SLIMCAT calculations. Atmospheric Chemistry and Physics, 16(16), 10501{10519.

Hegglin, M., Plummer, D., Shepherd, T., Scinocca, J., Anderson, J., Froidevaux, L., . . . others (2014). Vertical structure of stratospheric water vapour trends derived from merged satellite data. Nature Geoscience, 7(10), 768{776.

Hersbach, H., Bell, B., Berrisford, P., Hirahara, S., Hornyi, A., Muoz-Sabater, J., . . . Thpaut, J.-N. (2020). The ERA5 global reanalysis. Quarterly Journal of the Royal Meteorological Society, 146(730), 1999-2049. Retrieved from https://rmets.onlinelibrary.wiley.com/doi/abs/10.1002/qj.3803 doi: https://doi.org/10.1002/qj.3803

Holton, J. (2004). An introduction to dynamic meteorology (No. v. 1). Elsevier Academic Press. Retrieved from https://books.google.it/books?id=fhW5oDv3EPsC

Holton, J., & Choi, W.-K. (1988). Transport circulation deduced from sams trace species data. Journal of Atmospheric Sciences, 45(13), 1929{1939.

Hurrell, J. W., Holland, M. M., Gent, P. R., Ghan, S., Kay, J. E., Kushner, P. J., . . . others (2013). The community earth system model: a framework for collaborative research. Bulletin of the American Meteorological Society, 94(9), 1339{1360.

Jin, J. J., Semeniuk, K., Beagley, S. R., Fomichev, V. I., Jonsson, A. I., McConnell, J. C., . . . Dupuy, E. (2009). Comparison of cmam simulations of carbon monoxide (co), nitrous oxide (n_2o), and methane (ch_4) with observations from odin/smr, ace-fts, and aura/mls. Atmospheric Chemistry and Physics, 9(10), 3233{3252. Retrieved from https://acp.copernicus.org/articles/9/3233/2009/ doi: 10.5194/acp-9-3233-2009

Kobayashi, S., Ota, Y., Harada, Y., Ebita, A., Moriya, M., Onoda, H., . . . others (2015). The JRA-55 reanalysis: General speci cations and basic characteristics. Journal of the Meteorological Society of Japan. Ser. II, 93(1), 5{48.

Kolonjari, F., Plummer, D. A., Walker, K. A., Boone, C. D., Elkins, J. W., Hegglin, M. I., . . . Stiller, G. P. (2018). Assessing stratospheric transport in the cmam30 simulations using ace-fts measurements. Atmospheric Chemistry and Physics, 18(9), 6801{6828. Retrieved from https://acp.copernicus.org/articles/18/6801/2018/ doi: 10.5194/acp-18-6801-2018

Kyrölä, E., Laine, M., Sofieva, V., Tamminen, J., Päivärinta, S.-M., Tukiainen, S., . . . Thomason, L. (2013). Combined sage ii–gomos ozone profile data set for 1984–2011 and trend analysis of the vertical distribution of ozone. *Atmospheric Chemistry and Physics*, *13*(21), 10645–10658.

Laine, M., Latva-Pukkila, N., & Kyrölä, E. (2014). Analysing time-varying trends in stratospheric ozone time series using the state space approach. *Atmospheric Chemistry and Physics*, *14*(18), 9707–9725.

Langerock, B., De Mazière, M., Hendrick, F., Vigouroux, C., Desmet, F., Dils, B., & Niemeijer, S. (2015). Description of algorithms for co-locating and comparing gridded model data with remote-sensing observations. *Geoscientific Model Development*, *8*(3), 911–921. Retrieved from https://gmd.copernicus.org/articles/8/911/2015/ doi: 10.5194/gmd-8-911-2015

Lin, P., & Fu, Q. (2013). Changes in various branches of the Brewer–Dobson circulation from an ensemble of chemistry climate models. *Journal of Geophysical Research: Atmospheres*, *118*(1), 73–84.

Lin, S., & Rood, R. B. (1996). Multidimensional flux-form semi-lagrangian transport schemes. *Monthly Weather Review*, *124*(9), 2046–2070.

Lin, S.-J. (2004). A "vertically lagrangian" finite-volume dynamical core for global models. *Monthly Weather Review*, *132*(10), 2293–2307.

Linz, M., Plumb, R. A., Gupta, A., & Gerber, E. P. (2021). Stratospheric adiabatic mixing rates derived from the vertical gradient of age of air. *Journal of Geophysical Research: Atmospheres*, *126*(21), e2021JD035199.

Livesey, N. J., Read, W. G., Froidevaux, L., Lambert, A., Santee, M. L., Schwartz, M. J., . . . Nedoluha, G. E. (2021). Investigation and amelioration of long-term instrumental drifts in water vapor and nitrous oxide measurements from the aura microwave limb sounder (MLS) and their implications for studies of variability and trends. *Atmospheric Chemistry and Physics*, *21*(20), 15409–15430. Retrieved from https://acp.copernicus.org/articles/21/15409/2021/ doi: 10.5194/acp-21-15409-2021

Mahieu, E., Chipperfield, M., Notholt, J., Reddmann, T., Anderson, J., Bernath, P., . . . others (2014). Recent northern hemisphere stratospheric HCl increase due to atmospheric circulation changes. *Nature*, *515*(7525), 104.

Manney, G. L., & Hegglin, M. I. (2018). Seasonal and regional variations of long-term changes in upper-tropospheric jets from reanalyses. *Journal of Climate*, *31*(1), 423–448.

Marsh, D. R., Mills, M. J., Kinnison, D. E., Lamarque, J.-F., Calvo, N., & Polvani, L. M. (2013). Climate change from 1850 to 2005 simulated in cesm1(waccm). *Journal of Climate*, *26*(19), 7372 - 7391. Retrieved from https://journals.ametsoc.org/view/journals/clim/26/19/jcli-d-12-00558.1.xml doi: 10.1175/JCLI-D-12-00558.1

Matthes, K., Marsh, D. R., Garcia, R. R., Kinnison, D. E., Sassi, F., & Walters, S. (2010). Role of the qbo in modulating the influence of the 11 year solar cycle on the atmosphere using constant forcings. *Journal of Geophysical Research: Atmospheres*, *115*(D18).

Meinshausen, M., Nicholls, Z. R. J., Lewis, J., Gidden, M. J., Vogel, E., Freund, M., . . . Wang, R. H. J. (2020). The shared socio-economic pathway (ssp) greenhouse gas concentrations and their extensions to 2500. *Geoscientific Model Development*, *13*(8), 3571–3605. Retrieved from https://gmd.copernicus.org/articles/13/3571/2020/ doi: 10.5194/gmd-13-3571-2020

Meul, S., Dameris, M., Langematz, U., Abalichin, J., Kerschbaumer, A., Kubin, A., & Oberländer-Hayn, S. (2016). Impact of rising greenhouse gas concentrations on future tropical ozone and UV exposure. *Geophysical Research Letters*, *43*(6), 2919-2927. Retrieved from https://agupubs.onlinelibrary.wiley.com/doi/abs/10.1002/2016GL067997 doi: https://doi.org/10.1002/2016GL067997

Meul, S., Langematz, U., Kröger, P., Oberländer-Hayn, S., & Jöckel, P. (2018). Future changes in the stratosphere-to-troposphere ozone mass flux and the contribution from climate change and ozone recovery. Atmospheric Chemistry and Physics, 18(10), 7721–7738. Retrieved from https://acp.copernicus.org/articles/18/7721/2018/ doi: 10.5194/acp-18-7721-2018

Millán, L. F., Livesey, N. J., Santee, M. L., Neu, J. L., Manney, G. L., & Fuller, R. A. (2016). Case studies of the impact of orbital sampling on stratospheric trend detection and derivation of tropical vertical velocities: solar occultation vs. limb emission sounding. Atmospheric Chemistry and Physics, 16(18), 11521–11534. Retrieved from https://acp.copernicus.org/articles/16/11521/2016/ doi: 10.5194/acp-16-11521-2016

Mills, M. J., Richter, J. H., Tilmes, S., Kravitz, B., MacMartin, D. G., Glanville, A. A., ... Kinnison, D. E. (2017). Radiative and chemical response to interactive stratospheric sulfate aerosols in fully coupled cesm1(waccm). Journal of Geophysical Research: Atmospheres, 122(23), 13,061-13,078. Retrieved from https://agupubs.onlinelibrary.wiley.com/doi/abs/10.1002/2017JD027006 doi: https://doi.org/10.1002/2017JD027006

Minganti, D., Chabrillat, S., Christophe, Y., Errera, Q., Abalos, M., Prignon, M., ... Mahieu, E. (2020). Climatological impact of the Brewer–Dobson circulation on the N_2O budget in WACCM, a chemical reanalysis and a CTM driven by four dynamical reanalyses. Atmospheric Chemistry and Physics, 20(21), 12609–12631. Retrieved from https://acp.copernicus.org/articles/20/12609/2020/ doi: 10.5194/acp-20-12609-2020

Minganti, D., & Errera, Q. (2022). Supplement for: N_2O rate of change as a diagnostic of the brewer-dobson circulation in the stratosphere [dataset]. Royal Belgian Institute for Space Aeronomy. Retrieved from https://repository.aeronomie.be/?doi=10.18758/71021071 doi: https://dx.doi.org/10.18758/71021071

Minschwaner, K., Su, H., & Jiang, J. H. (2016). The upward branch of the brewer-dobson circulation quantified by tropical stratospheric water vapor and carbon monoxide measurements from the aura microwave limb sounder. Journal of Geophysical Research: Atmospheres, 121(6), 2790-2804. Retrieved from https://agupubs.onlinelibrary.wiley.com/doi/abs/10.1002/2015JD023961 doi: https://doi.org/10.1002/2015JD023961

Monge-Sanz, B. M., Chipperfield, M. P., Dee, D. P., Simmons, A. J., & Uppala, S. M. (2012). Improvements in the stratospheric transport achieved by a chemistry transport model with ECMWF (re)analyses: identifying effects and remaining challenges. Quarterly Journal of the Royal Meteorological Society, 139(672), 654-673. Retrieved from https://rmets.onlinelibrary.wiley.com/doi/abs/10.1002/qj.1996 doi: https://doi.org/10.1002/qj.1996

Morgenstern, O., Hegglin, M. I., Rozanov, E., O'Connor, F. M., Abraham, N. L., Akiyoshi, H., ... Zeng, G. (2017). Review of the global models used within phase 1 of the chemistry–climate model initiative (ccmi). Geoscientific Model Development, 10(2), 639–671. Retrieved from https://gmd.copernicus.org/articles/10/639/2017/ doi: 10.5194/gmd-10-639-2017

Neale, R. B., Richter, J., Park, S., Lauritzen, P. H., Vavrus, S. J., Rasch, P. J., & Zhang, M. (2013). The mean climate of the Community Atmosphere Model (CAM4) in forced SST and fully coupled experiments. Journal of Climate, 26(14), 5150–5168.

Nedoluha, G. E., Siskind, D. E., Lambert, A., & Boone, C. (2015). The decrease in mid-stratospheric tropical ozone since 1991. Atmospheric Chemistry and Physics, 15(8), 4215–4224. Retrieved from https://acp.copernicus.org/articles/15/4215/2015/ doi: 10.5194/acp-15-4215-2015

Oberländer-Hayn, S., Gerber, E. P., Abalichin, J., Akiyoshi, H., Kerschbaumer, A., Kubin, A., ... Oman, L. D. (2016). Is the Brewer-Dobson circulation increasing or moving upward? *Geophysical Research Letters*, *43*(4), 1772-1779. Retrieved from https://agupubs.onlinelibrary.wiley.com/doi/abs/10.1002/2015GL067545 doi: https://doi.org/10.1002/2015GL067545

Pisoft, P., Sacha, P., Polvani, L. M., Añel, J. A., De La Torre, L., Eichinger, R., . . . others (2021). Stratospheric contraction caused by increasing greenhouse gases. *Environmental Research Letters*, *16*(6), 064038.

Ploeger, F., Abalos, M., Birner, T., Konopka, P., Legras, B., Müller, R., & Riese, M. (2015). Quantifying the effects of mixing and residual circulation on trends of stratospheric mean age of air. *Geophysical Research Letters*, *42*(6), 2047–2054.

Ploeger, F., Diallo, M., Charlesworth, E., Konopka, P., Legras, B., Laube, J. C., . . . Riese, M. (2021). The stratospheric Brewer–Dobson circulation inferred from age of air in the ERA5 reanalysis. *Atmospheric Chemistry and Physics*, *21*(11), 8393–8412.

Ploeger, F., & Garny, H. (2022). Hemispheric asymmetries in recent changes in the stratospheric circulation. *Atmospheric Chemistry and Physics*, *22*(8), 5559–5576.

Ploeger, F., Legras, B., Charlesworth, E., Yan, X., Diallo, M., Konopka, P., . . . Riese, M. (2019). How robust are stratospheric age of air trends from different reanalyses? *Atmospheric Chemistry and Physics*, *19*(9), 6085–6105.

Plumb, R. A. (2002). Stratospheric transport. *Journal of the Meteorological Society of Japan. Ser. II*, *80*(4B), 793–809.

Plumb, R. A., & Ko, M. K. (1992). Interrelationships between mixing ratios of long-lived stratospheric constituents. *Journal of Geophysical Research: Atmospheres*, *97*(D9), 10145–10156.

Plummer, D., Nagashima, T., Tilmes, S., Archibald, A., Chiodo, G., Fadnavis, S., . . . others (2021). Ccmi-2022: A new set of chemistry-climate model initiative (ccmi) community simulations to update the assessment of models and support upcoming ozone assessment activities. *Newsletter n 57 July 2021*, 22.

Polvani, L. M., Wang, L., Abalos, M., Butchart, N., Chipperfield, M. P., Dameris, M., . . . Stone, K. A. (2019). Large Impacts, Past and Future, of Ozone-Depleting Substances on Brewer-Dobson Circulation Trends: A Multimodel Assessment. *Journal of Geophysical Research: Atmospheres*, *124*(13), 6669-6680. Retrieved from https://agupubs.onlinelibrary.wiley.com/doi/abs/10.1029/2018JD029516 doi: https://doi.org/10.1029/2018JD029516

Prather, M. J., Hsu, J., DeLuca, N. M., Jackman, C. H., Oman, L. D., Douglass, A. R., . . . others (2015). Measuring and modeling the lifetime of nitrous oxide including its variability. *Journal of Geophysical Research: Atmospheres*, *120*(11), 5693–5705.

Prignon, M., Chabrillat, S., Friedrich, M., Smale, D., Strahan, S., Bernath, P., . . . others (2021). Stratospheric fluorine as a tracer of circulation changes: comparison between infrared remote-sensing observations and simulations with five modern reanalyses. *Journal of Geophysical Research: Atmospheres*, e2021JD034995.

Prignon, M., Chabrillat, S., Minganti, D., O'Doherty, S., Servais, C., Stiller, G., . . . Mahieu, E. (2019). Improved FTIR retrieval strategy for HCFC-22 ($CHClF_2$), comparisons with in situ and satellite datasets with the support of models, and determination of its long-term trend above Jungfraujoch. *Atmospheric Chemistry and Physics Discussions*.

Randel, W., Boville, B. A., Gille, J. C., Bailey, P. L., Massie, S. T., Kumer, J., . . . Roche, A. (1994). Simulation of stratospheric N_2O in the NCAR CCM2: Comparison with CLAES data and global budget analyses. *Journal of the atmospheric sciences*, *51*(20), 2834–2845.

Randel, W., & Park, M. (2019). Diagnosing observed stratospheric water vapor relationships to the cold point tropical tropopause. *Journal of Geophysical Research: Atmospheres*, *124*(13), 7018–7033.

Rodgers, C. D. (2000). Inverse methods for atmospheric sounding: theory and practice (Vol. 2). World scientific.

Šacha, P., Eichinger, R., Garny, H., Pišoft, P., Dietmüller, S., de la Torre, L., ... others (2019). Extratropical age of air trends and causative factors in climate projection simulations. Atmospheric Chemistry and Physics, 19(11), 7627–7647.

Scaife, A., & James, I. (2000). Response of the stratosphere to interannual variability of tropospheric planetary waves. Quarterly Journal of the Royal Meteorological Society, 126(562), 275–297.

Seinfeld, J. H., & Pandis, S. N. (2016). Atmospheric chemistry and physics: from air pollution to climate change. John Wiley & Sons.

Sheese, P. E., Walker, K. A., Boone, C. D., Bernath, P. F., Froidevaux, L., Funke, B., ... von Clarmann, T. (2017). ACE-FTS ozone, water vapour, nitrous oxide, nitric acid, and carbon monoxide profile comparisons with MIPAS and MLS. Journal of Quantitative Spectroscopy and Radiative Transfer, 186, 63–80.

Shepherd, T. G. (2007). Transport in the middle atmosphere. Journal of the Meteorological Society of Japan. Ser. II, 85, 165–191.

Shepherd, T. G. (2008). Dynamics, stratospheric ozone, and climate change. Atmosphere-Ocean, 46(1), 117-138. Retrieved from https://doi.org/10.3137/ao.460106 doi: 10.3137/ao.460106

Simmons, A., Soci, C., Nicolas, J., Bell, B., Berrisford, P., Dragani, R., ... others (2020). Global stratospheric temperature bias and other stratospheric aspects of ERA5 and ERA5. 1. European Centre for Medium Range Weather Forecasts.

Stiller, G., Clarmann, T. v., Haenel, F., Funke, B., Glatthor, N., Grabowski, U., ... others (2012). Observed temporal evolution of global mean age of stratospheric air for the 2002 to 2010 period. Atmospheric Chemistry and Physics, 12(7), 3311–3331.

Stiller, G., Fierli, F., Ploeger, F., Cagnazzo, C., Funke, B., Haenel, F. J., ... Clarmann, T. v. (2017). Shift of subtropical transport barriers explains observed hemispheric asymmetry of decadal trends of age of air. Atmospheric Chemistry and Physics, 17(18), 11177–11192.

Strahan, S. E., Douglass, A., Stolarski, R., Akiyoshi, H., Bekki, S., Braesicke, P., ... others (2011). Using transport diagnostics to understand chemistry climate model ozone simulations. Journal of Geophysical Research: Atmospheres, 116(D17).

Strahan, S. E., Smale, D., Douglass, A. R., Blumenstock, T., Hannigan, J. W., Hase, F., ... others (2020). Observed hemispheric asymmetry in stratospheric transport trends from 1994 to 2018. Geophysical Research Letters, 47(17), e2020GL088567.

Strong, K., Wolff, M. A., Kerzenmacher, T. E., Walker, K. A., Bernath, P. F., Blumenstock, T., ... Wood, S. (2008). Validation of ACE-FTS N_2O measurements. Atmospheric Chemistry and Physics, 8(16), 4759–4786. Retrieved from https://acp.copernicus.org/articles/8/4759/2008/ doi: 10.5194/acp-8-4759-2008

Tian, H., Xu, R., Canadell, J. G., Thompson, R. L., Winiwarter, W., Suntharalingam, P., ... Yao, Y. (2020). A comprehensive quantification of global nitrous oxide sources and sinks. Nature, 586(7828), 248?256. doi: 10.1038/s41586-020-2780-0

von Clarmann, T., & Grabowski, U. (2021). Direct inversion of circulation from tracer measurements–Part 2: Sensitivity studies and model recovery tests. Atmospheric Chemistry and Physics, 21(4), 2509–2526.

Wargan, K., Orbe, C., Pawson, S., Ziemke, J. R., Oman, L. D., Olsen, M. A., ... Emma Knowland, K. (2018). Recent Decline in Extratropical Lower Stratospheric Ozone Attributed to Circulation Changes. Geophysical Research Letters, 45(10), 5166-5176. Retrieved from https://agupubs.onlinelibrary.wiley.com/doi/abs/10.1029/2018GL077406 doi: https://doi.org/10.1029/2018GL077406

Waugh, D., & Hall, T. (2002). Age of stratospheric air: Theory, observations, and models. Reviews of Geophysics, 40(4), 1{1.

Wolter, K., & Timlin, M. S. (2011). El Niño/Southern Oscillation behaviour since 1871 as diagnosed in an extended multivariate ENSO index (MEI. ext). International Journal of Climatology, 31(7), 1074{1087.

Xian, T., & Homeyer, C. R. (2019). Global tropopause altitudes in radiosondes and reanalyses. Atmospheric Chemistry and Physics, 19(8), 5661{5678.

Zander, R., Mahieu, E., Demoulin, P., Duchatelet, P., Roland, G., Servais, C., . . . Rinsland, C. (2008). Our changing atmosphere: Evidence based on long-term infrared solar observations at the jungfraujoch since 1950. Science of The Total Environment, 391(2), 184-195. Retrieved from https://www.sciencedirect.com/science/article/pii/S0048969707010789 (Research at Jungfraujoch - Contributions to the International conference in celebration of the 75th anniversary of the High Altitude Research Station Jungfraujoch at Interlaken, Switzerland (11-13 September, 2006)) doi: https://doi.org/10.1016/j.scitotenv.2007.10.018

Zhou, M., Langerock, B., Wells, K. C., Millet, D. B., Vigouroux, C., Sha, M. K., . . . De Mazière, M. (2019). An intercomparison of total column-averaged nitrous oxide between ground-based FTIR TCCON and NDACC measurements at seven sites and comparisons with the GEOS-Chem model. Atmospheric Measurement Techniques, 12(2), 1393{1408. Retrieved from https://amt.copernicus.org/articles/12/1393/2019/ doi: 10.5194/amt-12-1393-2019